East Asian Journal on Applied Mathematics
doi: 10.4208/eajam.2024-209.060525

Vol. **xx**, No. x, pp. 1-25
xxx 2026

A Time-Splitting Fourier-Collocation Method for Computing the Nonlinear Dirac Equation with Perfectly Matched Layers

Dandan Wang[1,2], Chunping Pang[3], Liping Wu[4]
and Hanquan Wang[5,*]

[1]*Eastern Institute for Advanced Study, Eastern Institute of Technology, Ningbo 315200, P.R. China.*
[2]*College of Mathematics, Sichuan University, Chengdu 610065, P.R. China.*
[3]*School of Statistics and Mathematics, Yunnan University of Finance and Economics, Kunming 650221, P.R. China.*
[4]*Faculty of Information Engineering and Automation, Kunming University of Science and Technology, Kunming 650500, P.R. China.*
[5]*Center for Applied Mathematics and School of Statistics and Mathematics, Yunnan University of Finance and Economics, Kunming 650221, P.R. China.*

Received 15 December 2024; Accepted (in revised version) 6 May 2025.

Abstract. This work is devoted to an efficient computation of the nonlinear Dirac (NLD) equation with perfectly matched layers (PML). When the PML is constructed, the Dirac operator in NLD equation has variable spatial coefficients. Direct application of the popular time-splitting Fourier spectral method to the equation with variable coefficients will cause numerical difficulties and lose the numerical accuracy. We introduce the time-splitting Fourier-collocation (TSFC) method to solve the problem. The Fourier-collocation method chooses the Fourier series-based functions as basis but the expansion coefficients are computed at a set of collocation points. Extensive numerical experimental results show that the TSFC method with PML can absorb efficiently the reflections to the edges of the computational region. Furthermore, the novel method is successfully applied to simulate the binary collision in one-dimensional NLD equation and to show the conical diffraction in honeycomb lattices described by two-dimensional NLD equation.

AMS subject classifications: 65M70, 78M22, 81-08

Key words: Nonlinear Dirac equation, perfectly matched layer, Fourier-collocation method, time-splitting method, conical diffraction.

1. Introduction

The Dirac equation plays an important role in particle physics and provides a description of the wave function for elementary spin-1/2 massive particles, such as electrons and

*Corresponding author. *Email addresses:* dandan95_wang@163.com (D. Wang), cppang1979@126.com (C. Pang), 554350754@qq.com (L. Wu), wang_hanquan@hotmail.com (H. Wang)

positrons. It is consistent both with the principle of the quantum mechanics and the theory of special relativity [22, 23]. Around 1970s and 1980s, the nonlinear Dirac equation with different self-interactions has been widely concerned in physics and mathematics — e.g. Thirring model [43], Soler model [42], Gross-Neveu model [29] and Bag model [36]. With the development of two-dimensional materials — e.g., graphene, quite recently, the Dirac equation has found profoundly new applications in investigating the structures of graphene [1, 6, 20, 27, 28, 37]. In honeycomb lattice, in certain cases, the nonlinear Dirac equation was derived to explore the nonlinear optical beam propagation in photonic crystals [4,24]. Additionally, the nonlinear Dirac equation was used in the study of the dynamics of topological insulators [2, 33].

When the Dirac equation is solved on a truncated domain, we have to avoid introducing artifacts into it and a regular approach is to use the truncation domain large enough to stay away from the boundary limits [5, 6, 12, 13, 18, 19, 25, 39–41, 44–46]. Although these methods have shown the efficiency and accuracy to one-dimensional NLD equation, it is challenging to solve high-dimensional problems on the large truncation regions. For example, the computation cost is quite expensive — i.e. in two-dimensional numerical computations [14, 26], the computation time $\approx$ 22 hours on 256 processors on the MAMMOUTH cluster for achieving a better numerical accuracy. Meanwhile, the same drawback exists in the numerical simulation of particle movement confined in intense laser fields [25, 39]. In order to overcome the outgoing wave reflected back at the boundary, several other efficient techniques have emerged in recent years. One efficient way is to introduce the absorbing boundary conditions to the system, so that we can get an accurate solution on the boundary of the Dirac equation [9]. Another efficient way is the perfectly matched layer method introduced by Berenger [15]. It shows that an absorbing boundary layer can be constructed to make the waves do not reflect at the interface when solving Maxwell equation. The PML method demonstrates superior absorption capabilities and has a low implementation cost for Maxwell, Schrödinger, and Dirac equations [8, 10, 16, 21]. When the PML technique is applied, the gradient terms in the NLD equation have variable coefficients which are piecewise-defined functions. Therefore, this equation cannot be efficiently solved by the popular time-splitting Fourier spectral (TSFS) method [12, 13]. To resolve this problem, Antoine *et al.* [7, 8] used the GMRES method along with a semi-implicit scheme. However, these methods still have several drawbacks. First, the use of an implicit scheme to treat the variable spatial coefficients complicates the implementation of the algorithm. Second, the method may suffer from a loss of accuracy and efficiency from a numerical perspective.

We propose an efficient time-splitting Fourier-collocation method for the Dirac-type equation with PML. The method employs Fourier series-based functions to make the corresponding expansion, with the expansion coefficients computed at selected collocation points. Numerical experiments show that:

(i) TSFC method has the spectral accuracy in space, whereas TSFS method does not show spectral convergence in space.

(ii) The PML obtained solution can absorb the reflection at the boundaries.

The paper is structured as follows. In Section 2, we reformulate the Soler model without electromagnetic interactions as an NLD equation and reduce it to a two-dimensional NLD equation and one-dimensional NLD equation. In Section 3, we apply the PML technique to one- and two-dimensional NLD equations. In Section 4, a TSFC method is used to efficiently discretize one- and two-dimensional NLD equations with PML. Extensive numerical results are presented in Section 5. Finally, conclusions are drawn in Section 6.

2. The Nonlinear Dirac Equation

In this paper, we pay attention to the NLD equation whose the nonlinearity is scalar self-interaction of Soler [42] and the model can be written in the following covariant form:

$$i\boldsymbol{\gamma}^{\mu}\partial_{\mu}\boldsymbol{\Psi} - m\boldsymbol{\Psi} + 2\lambda\left(\widetilde{\boldsymbol{\Psi}}\boldsymbol{\Psi}\right)\boldsymbol{\Psi} = 0, \tag{2.1}$$

where i is the imaginary unit — i.e. $i = \sqrt{-1}$, m a rest mass and $\lambda \in \mathbb{R}$ the interaction strength. Besides,

$$\boldsymbol{\gamma}^{\mu}\partial_{\mu}\boldsymbol{\Psi} = \sum_{\mu=0,1,2,3} \boldsymbol{\gamma}^{\mu}\partial_{\mu}\boldsymbol{\Psi},$$

and

$$\partial_0 = \partial/(c\partial t), \quad \partial_j = \partial/\partial x_j, \quad j = 1,2,3$$

are the covariant derivatives. The complex-valued vector wave function $\boldsymbol{\Psi} = (\Psi_1, \Psi_2, \Psi_3, \Psi_4)^T \in \mathbb{C}^4$, $\boldsymbol{\Psi}^{\dagger}$ is the complex conjugate transpose of $\boldsymbol{\Psi}$, $\widetilde{\boldsymbol{\Psi}} = \boldsymbol{\Psi}^{\dagger}\boldsymbol{\gamma}^{\mathbf{0}}$ the adjoint spinor, and $\boldsymbol{\gamma}^{\mu}$, $\mu = 0,1,2,3$ are 4×4 matrices defined by

$$\boldsymbol{\gamma}^{\mathbf{0}} = \begin{pmatrix} \boldsymbol{I} & \mathbf{0} \\ \mathbf{0} & -\boldsymbol{I} \end{pmatrix}, \quad \boldsymbol{\gamma}^{j} = \begin{pmatrix} \mathbf{0} & \boldsymbol{\sigma}_j \\ -\boldsymbol{\sigma}_j & \mathbf{0} \end{pmatrix}, \quad j = 1,2,3,$$

where $\boldsymbol{I}$ and $\mathbf{0}$ are respectively 2×2 unit and null matrices, and

$$\boldsymbol{\sigma}_{\mathbf{1}} = \begin{pmatrix} 0 & 1 \\ 1 & 0 \end{pmatrix}, \quad \boldsymbol{\sigma}_{\mathbf{2}} = \begin{pmatrix} 0 & -i \\ i & 0 \end{pmatrix}, \quad \boldsymbol{\sigma}_{\mathbf{3}} = \begin{pmatrix} 1 & 0 \\ 0 & -1 \end{pmatrix}$$

are the Pauli matrices.

Multiplying both sides of the Eq. (2.1) by $(-i)$ gives

$$\boldsymbol{\gamma}^{\mathbf{0}}\partial_0\boldsymbol{\Psi} = -\sum_{j=1}^{3}\boldsymbol{\gamma}^{j}\partial_j\boldsymbol{\Psi} - i\left(m - 2\lambda\boldsymbol{\Psi}^{\dagger}\boldsymbol{\gamma}^{\mathbf{0}}\boldsymbol{\Psi}\right)\boldsymbol{\Psi}. \tag{2.2}$$

We note that $\boldsymbol{\beta} = \boldsymbol{\gamma}^0$, $\boldsymbol{\alpha}_j = \boldsymbol{\gamma}^{\mathbf{0}}\boldsymbol{\gamma}^{j}$, $j = 1,2,3$ are the 4×4 Dirac matrices defined as

$$\boldsymbol{\beta} = \begin{pmatrix} \boldsymbol{I} & \mathbf{0} \\ \mathbf{0} & -\boldsymbol{I} \end{pmatrix}, \quad \boldsymbol{\alpha}_j = \begin{pmatrix} \mathbf{0} & \boldsymbol{\sigma}_j \\ \boldsymbol{\sigma}_j & \mathbf{0} \end{pmatrix}, \quad j = 1,2,3. \tag{2.3}$$

Substituting (2.3) into (2.2), we obtain the following NLD equation in three dimension with $c = 1$ [32,46]:

$$\partial_t \boldsymbol{\Psi} = -\left(\sum_{j=1}^{3} \boldsymbol{\alpha_j}\, \partial_{x_j}\right) \boldsymbol{\Psi} - if\left(\boldsymbol{\Psi}^\dagger \boldsymbol{\beta} \boldsymbol{\Psi}\right) \boldsymbol{\beta} \boldsymbol{\Psi}, \tag{2.4}$$

where

$$\boldsymbol{\Psi} = \boldsymbol{\Psi}(\boldsymbol{x}, t) = \big(\Psi_1(\boldsymbol{x}, t), \Psi_2(\boldsymbol{x}, t), \Psi_3(\boldsymbol{x}, t), \Psi_4(\boldsymbol{x}, t)\big)^T$$

is the wave function, t the time variable, and $\boldsymbol{x} = (x_1, x_2, x_3) \in \mathbb{R}^3$ are the spatial coordinates. The nonlinearity is controlled by the real-valued function $f(s) = m - 2\lambda s$ with $s = \boldsymbol{\Psi}^\dagger \boldsymbol{\beta} \boldsymbol{\Psi}$.

Making the dimension reduction similar to [11], when the initial data $\boldsymbol{\Psi}(\boldsymbol{x}, t = 0)$ is independent of x_3, we formally assume the wave function $\boldsymbol{\Psi}$ is concentrated on the x_1x_2-plane, then the three-dimensional (3D) NLD equation (2.4) can be reduced to the NLD equation in two dimension — i.e.

$$\partial_t \boldsymbol{\Psi} = -\left(\sum_{j=1}^{2} \boldsymbol{\alpha_j}\, \partial_{x_j}\right) \boldsymbol{\Psi} - if\left(\boldsymbol{\Psi}^\dagger \boldsymbol{\beta} \boldsymbol{\Psi}\right) \boldsymbol{\beta} \boldsymbol{\Psi}, \tag{2.5}$$

where

$$\boldsymbol{\Psi} = \boldsymbol{\Psi}(\boldsymbol{x}, t) = \big(\Psi_1(\boldsymbol{x}, t), \Psi_2(\boldsymbol{x}, t), \Psi_3(\boldsymbol{x}, t), \Psi_4(\boldsymbol{x}, t)\big)^T, \quad \boldsymbol{x} = (x_1, x_2) \in \mathbb{R}^2.$$

Similarly, the three-dimensional NLD equation (2.4) can be reduced to the one-dimensional NLD equation

$$\partial_t \boldsymbol{\Psi} = -\boldsymbol{\sigma_1} \partial_{x_1} \boldsymbol{\Psi} - if\big(|\Psi_1|^2 - |\Psi_2|^2\big)\boldsymbol{\sigma_3} \boldsymbol{\Psi}, \tag{2.6}$$

where

$$\boldsymbol{\Psi} = \boldsymbol{\Psi}(x_1, t) = \big(\Psi_1(x_1, t), \Psi_2(x_1, t)\big)^T, \quad x_1 \in \mathbb{R}.$$

The NLD equation (2.4) has several good conservative properties, such as the conservation of the total mass (or the total charge, or the total linear momentum or the total energy). The more detailed information can be found in [31].

3. Nonlinear Dirac Equation with PML

The NLD equation is often solved on a finite domain with appropriate conditions specified on the domain boundary. For example, in numerical simulations of semi-conductors, it is crucial to allow the electron flow across the device and to avoid unphysical reflections at the boundary of the numerical domain [38]. One way to solve the problem is the using of PML technique. We apply the same PML approach as in [48] to one- and two-dimensional NLD equations, and use $\mathscr{D}_{phy}$ to denote the truncated physical domain.

3.1. A one-dimensional nonlinear Dirac equation with PML

Based on (2.6), we consider the initial-boundary value problem for the one-dimensional NLD equation

$$\begin{aligned}
&\partial_t \mathbf{\Psi} = \left[-\boldsymbol{\sigma_1}\partial_{x_1} - if\left(|\Psi_1|^2 - |\Psi_2|^2\right)\boldsymbol{\sigma}_3\right]\mathbf{\Psi}, \quad x_1 \in \mathscr{D}_{phy}, \quad 0 \le t \le T,\\
&\mathbf{\Psi}(x_{1,L}, t) = \mathbf{\Psi}(x_{1,R}, t), \qquad\qquad\qquad\qquad\qquad\quad 0 \le t \le T,\\
&\mathbf{\Psi}(x_1, t=0) = \mathbf{\Psi}^0(x_1), \qquad\qquad\qquad\quad x_1 \in \overline{\mathscr{D}}_{phy}.
\end{aligned}$$

With the help of PML technique, we are going to solve the following problem:

$$\partial_t \mathbf{\Psi} = \left[-\boldsymbol{\sigma_1} c_1(x_1)\partial_{x_1} - if\left(|\Psi_1|^2 - |\Psi_2|^2\right)\boldsymbol{\sigma}_3\right]\mathbf{\Psi}, \quad x_1 \in \mathscr{D}, \quad 0 \le t \le T, \tag{3.1}$$

$$\mathbf{\Psi}\left(x_{1,L}^*, t\right) = \mathbf{\Psi}\left(x_{1,R}^*, t\right), \qquad 0 \le t \le T, \tag{3.2}$$

$$\mathbf{\Psi}(x_1, t=0) = \mathbf{\Psi}^0(x_1), \qquad x_1 \in \overline{\mathscr{D}}, \tag{3.3}$$

where $c_1(x_1) = 1/(1+e^{i\theta_1}\widetilde{\sigma}_1(x_1))$ and it is equal to 1 when $x_1 \in \mathscr{D}_{phy}$. The incidence angle $\theta_1 \in (0, \pi/2)$ and the absorbing function $\widetilde{\sigma}_1$ has the form

$$\widetilde{\sigma}_1(x_1) = \begin{cases} \sigma\left(x_{1,L}^* - x_1\right), & x_{1,L}^* \le x_1 < x_{1,L},\\ 0, & x_{1,L} \le x_1 \le x_{1,R},\\ \sigma\left(x_1 - x_{1,R}^*\right), & x_{1,R} < x_1 \le x_{1,R}^*. \end{cases}$$

Here, we add a layer surrounding the physical domain $\mathscr{D}_{phy} = (x_{1,L}, x_{1,R})$ and consider a lager domain

$$\mathscr{D} = \overline{\mathscr{D}_{phy}} \bigcup \mathscr{D}_{PML} = \left(x_{1,L}^*, x_{1,R}^*\right),$$

cf. Fig. 1.

How we can get the one-dimensional NLD equation with PML — i.e. Eqs. (3.1)-(3.3)? Here we briefly introduce the idea. In fact, to avoid the outgoing wave reflected back at the boundary, typical PML technique adds a layer around the original computational domain $\mathscr{D}_{phy}$ and applies a complex coordinate transform to the original equation — i.e.

$$x_1 \;\rightarrow\; x_1 + e^{i\theta_1}\left(\int_{x_{1,L}}^{x_1} \sigma(s)\,ds + \int_{x_{1,R}}^{x_1} \sigma(s)\,ds\right), \quad x_1 \in \overline{\mathscr{D}}.$$

Here, $\sigma(s)$ is a continuous, positive, non-decreasing function such that $\sigma(s) = 0$ for $s \in \mathscr{D}_{phy}$. Then by some mathematical deduction, one may obtain the Eqs. (3.1)-(3.3).

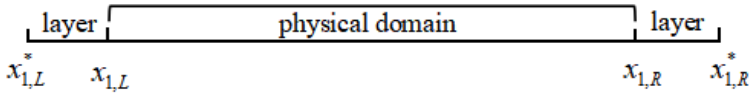

Figure 1: A PML in one-dimensional system.

3.2. Two-dimensional nonlinear Dirac equation with PML

Similarly, in two-dimensional problems, we add a layer surrounding the physical domain $\mathscr{D}_{phy}$, and the computational domain is chosen as

$$\mathscr{D} = \overline{\mathscr{D}_{phy}} \bigcup \mathscr{D}_{PML} = \left(x^*_{1,L}, x^*_{1,R}\right) \times \left(x^*_{2,L}, x^*_{2,R}\right),$$

cf. Fig. 2, where $\mathscr{D}_{PML}$ is the blue shaded area.

We consider the following two-dimensional NLD equation with PML [48]:

$$\partial_t \boldsymbol{\Psi} = -\left(\sum_{j=1}^{2} \boldsymbol{\alpha_j} c_j(x_j)\, \partial_{x_j}\right) \boldsymbol{\Psi} - if\left(\boldsymbol{\Psi}^\dagger \boldsymbol{\beta} \boldsymbol{\Psi}\right) \boldsymbol{\beta} \boldsymbol{\Psi}, \quad (x_1, x_2) \in \mathscr{D}, \quad 0 \le t \le T, \tag{3.4}$$

$$\boldsymbol{\Psi}(x_1, x_2, t) \text{ is periodic}, \quad (x_1, x_2) \in \partial\overline{\mathscr{D}}, \quad 0 \le t \le T, \tag{3.5}$$

$$\boldsymbol{\Psi}(x_1, x_2, t=0) = \boldsymbol{\Psi}^0(x_1, x_2), \quad (x_1, x_2) \in \overline{\mathscr{D}}, \tag{3.6}$$

where $c_j(x_j) = 1/(1 + e^{i\theta_j}\widetilde{\sigma}_j(x_j))$, $j = 1, 2$ and it is equal to 1 when $x_j \in (x_{j,L}, x_{j,R})$. The incidence angle $\theta_j \in (0, \pi/2)$ and the absorbing function $\widetilde{\sigma}$ has the form

$$\widetilde{\sigma}_j(x_j) = \begin{cases} \sigma(x^*_{j,L} - x_j), & x^*_{j,L} \le x_j < x_{j,L}, \\ 0, & x_{j,L} \le x_j \le x_{j,R}, \\ \sigma(x_j - x^*_{j,R}), & x_{j,R} < x_j \le x^*_{j,R}, \end{cases} \quad \text{for} \quad j = 1, 2.$$

In the upcoming section, we will introduce a novel numerical method to solve the Eqs. (3.1)-(3.3) and (3.4)-(3.6).

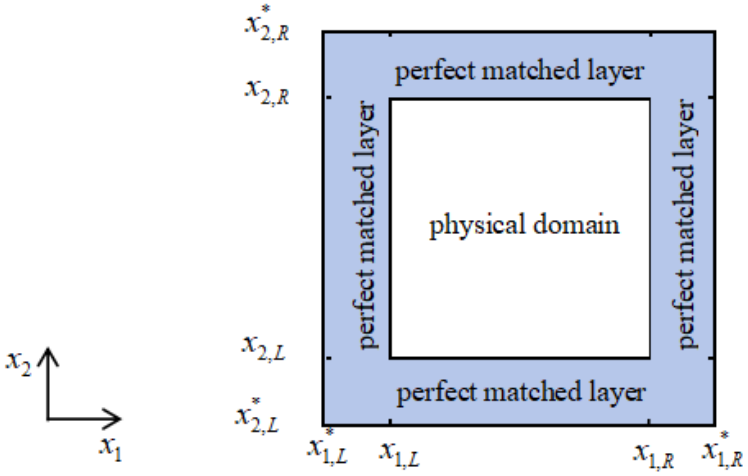

Figure 2: A PML in two dimensional system.

4. A Time-Splitting Fourier-Collocation Method

We use a time-splitting method to the NLD equation and hope the equation can be solved with a lower cost. There are many kinds of time-splitting methods, such as the first-order Lie-Trotter splitting method, the second-order Strang splitting method and many other higher-order splitting methods [30, 47]. Under the first-order time-splitting technique, the NLD equation can be split into two simpler parts: the linear equation and the nonlinear equation. The former one can be efficiently solved by the Fourier-collocation (FC) method in space and the nonlinear one can be computed exactly.

4.1. An introduction to the Fourier-collocation method

There are several ways to show the FC method, and here we show how to evaluate the first-order derivative of a periodic function defined on $[0,2\pi]$ by the FC method. Let the unknown periodic function $u(x)$ is defined on $[0,2\pi]$, so we choose $x_j = 2\pi j/N$, $j = 0,1,\ldots,N-1$ as collocation points. We assume that

$$u(x) \approx u_N(x) = \sum_{j=0}^{N-1} u(x_j) L_j(x), \quad x \in [0,2\pi], \tag{4.1}$$

where $N > 0$ is some known integer. The Lagrangian interpolation function

$$L_j(x) = 1/N \sin[N(x-x_j)/2] \cot[(x-x_j)/2]$$

satisfies the interpolation property

$$L_j(x_k) = \begin{cases} 1, & j = k, \\ 0, & j \neq k. \end{cases} \tag{4.2}$$

Furthermore, we can derive the first-order derivative of $u_N(x)$, viz.

$$du_N(x)/dx = \sum_{j=0}^{N-1} u(x_j)\, dL_j(x)/dx.$$

Using the FC method, we approximate the first-order derivative of $u(x)$ at grid points x_k, $k = 0,\ldots,N-1$ as

$$du(x)/dx\,\big|_{x=x_k} \approx du_N(x)/dx\,\big|_{x=x_k} = \sum_{j=0}^{N-1} d_{k,j}\, u(x_j),$$

where the first-order differentiation matrix $D = \{d_{kj}\}_{k,j=0}^{N-1}$ has the form

$$d_{kj} = dL_j(x)/dx\,\big|_{x=x_k} = \begin{cases} 1/2(-1)^{k+j} \cot[(k-j)\pi/N], & k \neq j, \\ 0, & k = j. \end{cases}$$

In what follows, we use the time-splitting and FC methods to solve one- and two-dimensional NLD equations with PML.

4.2. Discretization of one-dimensional nonlinear Dirac equation

According to the Lie-Trotter time-splitting technique, we can split the Eq. (3.1) into two equations — viz.

$$\partial_t \mathbf{\Psi}(x_1,t) = -\boldsymbol{\sigma_1} c_1(x_1)\partial_{x_1}\mathbf{\Psi}(x_1,t) =: \mathscr{A}\mathbf{\Psi}(x_1,t), \qquad x_1 \in \mathscr{D}, \tag{4.3}$$

$$\partial_t \mathbf{\Psi}(x_1,t) = -if\left(|\Psi_1|^2 - |\Psi_2|^2\right)\boldsymbol{\sigma}_3\mathbf{\Psi}(x_1,t) =: \mathscr{B}\mathbf{\Psi}(x_1,t), \quad x_1 \in \mathscr{D}, \tag{4.4}$$

where

$$\mathbf{\Psi}(x_1,t) = \big(\Psi_1(x_1,t), \Psi_2(x_1,t)\big)^T$$

is the wave function, $\mathscr{D} = (x^*_{1,L}, x^*_{1,R})$ the computational domain, and $t \in [0,T]$ the time variable. Note that $\mathscr{A}$ is a linear operator and $\mathscr{B}$ a nonlinear one. We choose a spatial mesh size $h_1 = (x^*_{1,R} - x^*_{1,L})/N_1 > 0$ and time step $\triangle t = T/M$, where N_1 and M are positive integers, and define grid points as

$$x_{1,k_1} = x^*_{1,L} + k_1 h_1, \quad k_1 = 0,1,\ldots,N_1, \quad t_n = n\triangle t, \quad n = 0,1,\ldots,M.$$

Let $\Psi^n_{1,k_1} \approx \Psi_1(x_{1,k_1},t_n)$ and $\Psi^n_{2,k_1} \approx \Psi_2(x_{1,k_1},t_n)$, and the solution vector $\mathbf{\Psi}^n_{\mathbf{1}} = \{\Psi^n_{1,k_1}\}^{N_1-1}_{k_1=0}$, $\mathbf{\Psi}^n_{\mathbf{2}} = \{\Psi^n_{2,k_1}\}^{N_1-1}_{k_1=0}$.

Remark 4.1. While using the Lie-Trotter splitting method for solving the Eqs. (3.1)-(3.3) in time, we can compactly express the approximate solution $\mathbf{\Psi}^I$ as the composition of two flows, viz.

$$\mathbf{\Psi}^I = \mathbf{\Psi}^{\mathscr{B}}_{\triangle t} \circ \mathbf{\Psi}^{\mathscr{A}}_{\triangle t},$$

where $\mathbf{\Psi}^{\mathscr{A}}_{\triangle t}$ denotes the approximate flow to the linear part (4.3), and $\mathbf{\Psi}^{\mathscr{B}}_{\triangle t}$ is the exact flow of the nonlinear part (4.4).

4.3. Fourier-collocation discretization of linear equation (4.3) in space

We apply the FC method to discretize the linear part in space. Using the notations of [8], we diagonalize the Pauli matrix $\boldsymbol{\sigma}_1 = \mathbf{\Pi}\mathbf{\Lambda}\mathbf{\Pi}^\dagger$, where

$$\mathbf{\Lambda} = \begin{pmatrix} -1 & 0 \\ 0 & 1 \end{pmatrix}, \quad \mathbf{\Pi} = 1/\sqrt{2}\begin{pmatrix} -1 & 1 \\ 1 & 1 \end{pmatrix}, \quad \mathbf{\Pi}^\dagger = 1/\sqrt{2}\begin{pmatrix} -1 & 1 \\ 1 & 1 \end{pmatrix}.$$

Taking into account this factorization, we get

$$\Phi_1 = -1/\sqrt{2}\Psi_1 + 1/\sqrt{2}\Psi_2, \quad \Phi_2 = 1/\sqrt{2}\Psi_1 + 1/\sqrt{2}\Psi_2,$$

and decouple the Eq. (4.3) as

$$\partial_t \Phi_1 = c_1(x_1)\partial_{x_1}\Phi_1, \quad \partial_t \Phi_2 = -c_1(x_1)\partial_{x_1}\Phi_2, \tag{4.5}$$

where $\Phi_1 = \Phi_1(x_1,t), \Phi_2 = \Phi_2(x_1,t)$ are unknown functions.

Similar to (4.1), we approximate $\Phi_1(x_1,t)$ and $\Phi_2(x_1,t)$ as

$$\Phi_\eta(x_1,t) \approx \Phi_{\eta,N_1}(x_1,t) = \sum_{j_1=0}^{N_1-1} \Phi_{\eta,j_1}(t)\, L_{j_1}(\overline{x}_1), \quad \eta = 1,2, \tag{4.6}$$

where

$$\overline{x}_1 = 2\pi(x_1 - x^*_{1,L})/(x^*_{1,R} - x^*_{1,L}) \in [0, 2\pi].$$

Substituting (4.6) into (4.5), we collocate the obtained equations at the grid points $x_1 = x_{1,k_1}$, $k_1 = 0,1,\ldots,N_1-1$ and consider the interpolation property (4.2) at the same time. As a result, we obtain the following discrete ODEs for Φ_1 and Φ_2:

$$\begin{aligned} \partial_t \Phi_{1,k_1}(t) &= \gamma c_1(x_{1,k_1}) \sum_{j_1=0}^{N_1-1} d_{k_1,j_1} \Phi_{1,j_1}(t), \qquad k_1 = 0,1,\ldots,N_1-1, \\ \partial_t \Phi_{2,k_1}(t) &= -\gamma c_1(x_{1,k_1}) \sum_{j_1=0}^{N_1-1} d_{k_1,j_1} \Phi_{2,j_1}(t), \quad k_1 = 0,1,\ldots,N_1-1 \end{aligned} \tag{4.7}$$

with $\gamma = 2\pi/(x^*_{1,R} - x^*_{1,L})$. Introducing the first derivative matrix $\boldsymbol{D} = \{d_{k_1,j_1}\}_{k_1,j_1=0}^{N_1-1}$, we write (4.7) in the matrix form

$$\partial_t \boldsymbol{\Phi_1} = \gamma \boldsymbol{G} \boldsymbol{\Phi_1}, \quad \partial_t \boldsymbol{\Phi_2} = -\gamma \boldsymbol{G} \boldsymbol{\Phi_2} \tag{4.8}$$

with unknown vectors $\boldsymbol{\Phi_1} = \boldsymbol{\Phi_1}(t) = \{\Phi_{1,k_1}(t)\}_{k_1=0}^{N_1-1}$, $\boldsymbol{\Phi_2} = \boldsymbol{\Phi_2}(t) = \{\Phi_{2,k_1}(t)\}_{k_1=0}^{N_1-1}$, and $N_1 \times N_1$ coefficient matrix $\boldsymbol{G} = \boldsymbol{C}\boldsymbol{D}$, where

$$\boldsymbol{C} = \operatorname{diag}\big(c_1(x_{1,0}), c_1(x_{1,1}), \ldots, c_1(x_{1,N_1-1})\big).$$

Since the coefficient matrix $\boldsymbol{G}$ has N_1 linearly independent eigenvectors, there exists an invertible matrix $\boldsymbol{P}$ such that $\boldsymbol{G} = \boldsymbol{P}\boldsymbol{\lambda}\boldsymbol{P}^{-1}$ with $\boldsymbol{\lambda} = \operatorname{diag}(\lambda_0, \lambda_1, \ldots, \lambda_{N_1-1})$. Therefore,

$$\begin{pmatrix} \boldsymbol{\phi_1} \\ \boldsymbol{\phi_2} \end{pmatrix} = \begin{pmatrix} \boldsymbol{P^{-1}\Phi_1} \\ \boldsymbol{P^{-1}\Phi_2} \end{pmatrix},$$

and the Eq. (4.8) can be converted to the following ODEs:

$$\partial_t \boldsymbol{\phi_1} = \gamma \boldsymbol{\lambda} \boldsymbol{\phi_1}, \quad \partial_t \boldsymbol{\phi_2} = -\gamma \boldsymbol{\lambda} \boldsymbol{\phi_2} \tag{4.9}$$

for vectors $\boldsymbol{\phi_1} = \boldsymbol{\phi_1}(t) = \{\phi_{1,k_1}(t)\}_{k_1=0}^{N_1-1}$, $\boldsymbol{\phi_2} = \boldsymbol{\phi_2}(t) = \{\phi_{2,k_1}(t)\}_{k_1=0}^{N_1-1}$. The components of Eq. (4.9) can be written as

$$\begin{aligned} \partial_t \phi_{1,k_1} &= \gamma \lambda_{k_1} \phi_{1,k_1}, \qquad k_1 = 0,1,\ldots,N_1-1, \\ \partial_t \phi_{2,k_1} &= -\gamma \lambda_{k_1} \phi_{2,k_1}, \qquad k_1 = 0,1,\ldots,N_1-1. \end{aligned} \tag{4.10}$$

The Eqs. (4.10) can be solved exactly for the time from $t = t_n$ to $t = t_{n+1}$, so that

$$\begin{aligned}\phi_{1,k_1}^{n+1} &= e^{\gamma\lambda_{k_1}\triangle t}\phi_{1,k_1}^{n}, \quad 0 \le k_1 \le N_1-1, \quad 0 \le n \le M-1,\\ \phi_{2,k_1}^{n+1} &= e^{-\gamma\lambda_{k_1}\triangle t}\phi_{2,k_1}^{n}, \quad 0 \le k_1 \le N_1-1, \quad 0 \le n \le M-1.\end{aligned} \tag{4.11}$$

We denote the solution vectors by $\boldsymbol{\phi}_{\mathbf{1}}^{n+1} = \{\phi_{1,k_1}^{n+1}\}_{k_1=0}^{N_1-1}$, $\boldsymbol{\phi}_{\mathbf{2}}^{n+1} = \{\phi_{2,k_1}^{n+1}\}_{k_1=0}^{N_1-1}$. Using the Eqs. (4.5), (4.8), (4.9), and (4.11), we get the numerical solution of the Eq. (4.3), viz.

$$\begin{aligned}\boldsymbol{\Psi}_{\mathbf{1}}^{n+1} &= -1/\sqrt{2}\boldsymbol{P}\boldsymbol{\phi}_{\mathbf{1}}^{n+1} + 1/\sqrt{2}\boldsymbol{P}\boldsymbol{\phi}_{\mathbf{2}}^{n+1},\\ \boldsymbol{\Psi}_{\mathbf{2}}^{n+1} &= 1/\sqrt{2}\boldsymbol{P}\boldsymbol{\phi}_{\mathbf{1}}^{n+1} + 1/\sqrt{2}\boldsymbol{P}\boldsymbol{\phi}_{\mathbf{2}}^{n+1},\end{aligned}$$

where $\boldsymbol{\Psi}_{\mathbf{1}}^{n+1} = \{\Psi_{1,k_1}^{n+1}\}_{k_1=0}^{N_1-1}$ and $\boldsymbol{\Psi}_{\mathbf{2}}^{n+1} = \{\Psi_{2,k_1}^{n+1}\}_{k_1=0}^{N_1-1}$.

4.4. Exact solution of nonlinear equation (4.4)

From the nonlinear part,

$$\partial_t\boldsymbol{\Psi}(x_1,t) = -if\left(|\Psi_1|^2-|\Psi_2|^2\right)\boldsymbol{\sigma}_3\boldsymbol{\Psi}(x_1,t), \quad t\in[t_n,t_{n+1}]$$

and its complex conjugate

$$\partial_t\overline{\boldsymbol{\Psi}}(x_1,t) = if\left(|\Psi_1|^2-|\Psi_2|^2\right)\boldsymbol{\sigma}_3\overline{\boldsymbol{\Psi}}(x_1,t), \quad t\in[t_n,t_{n+1}]$$

we conclude that

$$\partial_t|\boldsymbol{\Psi}(x_1,t)|^2 = \partial_t\left(\boldsymbol{\Psi}(x_1,t)\overline{\boldsymbol{\Psi}}(x_1,t)\right) = \mathbf{0}, \quad t\in[t_n,t_{n+1}].$$

This means that $|\boldsymbol{\Psi}(x_1,t)|^2 = |\boldsymbol{\Psi}(x_1,t_n)|^2$ for all $t\in[t_n,t_{n+1}]$. Therefore, the nonlinear equation can be transformed into a simple ODEs, viz.

$$\partial_t\boldsymbol{\Psi}(x_1,t) = -if\left(|\Psi_1(x_1,t_n)|^2-|\Psi_2(x_1,t_n)|^2\right)\boldsymbol{\sigma}_3\boldsymbol{\Psi}(x_1,t).$$

The above ODEs on $[t_n,t_{n+1}]$ can be solved exactly and obtain the following solutions for any k_1:

$$\begin{aligned}\Psi_{1,k_1}^{n+1} &= e^{-if(|\Psi_{1,k_1}^n|^2-|\Psi_{2,k_1}^n|^2)\triangle t}\Psi_{1,k_1}^n, \quad k_1 = 0,1,\ldots,N_1-1,\\ \Psi_{2,k_1}^{n+1} &= e^{if(|\Psi_{1,k_1}^n|^2-|\Psi_{2,k_1}^n|^2)\triangle t}\Psi_{2,k_1}^n, \quad k_1 = 0,1,\ldots,N_1-1.\end{aligned}$$

We summarize the procedure for solving the one-dimensional equation (3.1) in Algorithm 4.1.

Algorithm 4.1 Time-Splitting Fourier-Collocation Method for 1D System (3.1)

1: Given initial values $\boldsymbol{\Psi}_{\mathbf{1}}^0 = \{\Psi_1(x_{1,k_1},0)\}_{k_1=0}^{N_1}, \boldsymbol{\Psi}_{\mathbf{2}}^0 = \{\Psi_2(x_{1,k_1},0)\}_{k_1=0}^{N_1}$.
2: $M = T/\triangle t$, $\triangle t$ is the time step.

3: Let the Pauli matrix $\boldsymbol{\sigma}_1$ be factorized into $\boldsymbol{\Pi}\boldsymbol{\Lambda}\boldsymbol{\Pi}^\dagger$ and find coefficient matrix $\boldsymbol{G} = \boldsymbol{P}\boldsymbol{\lambda}\boldsymbol{P}^{-1}$ with $\boldsymbol{\lambda} = \mathrm{diag}(\lambda_0, \lambda_1, \ldots, \lambda_{N_1-1})$.

4: **for** $n = 0 : M-1$ **do**

5: Get

$$\boldsymbol{\Phi}_1^n = -1/\sqrt{2}\boldsymbol{\Psi}_1^n + 1/\sqrt{2}\boldsymbol{\Psi}_2^n, \quad \boldsymbol{\Phi}_2^n = 1/\sqrt{2}\boldsymbol{\Psi}_1^n + 1/\sqrt{2}\boldsymbol{\Psi}_2^n.$$

6: Calculate

$$\boldsymbol{\Phi}_1^* = \boldsymbol{P}e^{\gamma\boldsymbol{\lambda}\triangle t}\boldsymbol{P}^{-1}\boldsymbol{\Phi}_1^n, \quad \boldsymbol{\Phi}_2^* = \boldsymbol{P}e^{-\gamma\boldsymbol{\lambda}\triangle t}\boldsymbol{P}^{-1}\boldsymbol{\Phi}_2^n.$$

7: Compute

$$\boldsymbol{\Psi}_1^* = -1/\sqrt{2}\boldsymbol{\Phi}_1^* + 1/\sqrt{2}\boldsymbol{\Phi}_2^*, \quad \boldsymbol{\Psi}_2^* = 1/\sqrt{2}\boldsymbol{\Phi}_1^* + 1/\sqrt{2}\boldsymbol{\Phi}_2^*.$$

8: Obtain $\boldsymbol{\Psi}_1^{n+1}$ and $\boldsymbol{\Psi}_2^{n+1}$ from

$$\Psi_{1,k_1}^{n+1} = e^{-if(|\Psi_{1,k_1}^*|^2 - |\Psi_{2,k_1}^*|^2)\triangle t}\Psi_{1,k_1}^*, \quad k_1 = 0, 1, \ldots, N_1 - 1,$$
$$\Psi_{2,k_1}^{n+1} = e^{if(|\Psi_{1,k_1}^*|^2 - |\Psi_{2,k_1}^*|^2)\triangle t}\Psi_{2,k_1}^*, \quad k_1 = 0, 1, \ldots, N_1 - 1.$$

9: **end for**

Remark 4.2. In order to get a better numerical approximation in time, we may apply the following second-order time-splitting method:

$$\boldsymbol{\Psi}^{II} = \boldsymbol{\Psi}_{\triangle t/2}^{\mathscr{B}} \circ \boldsymbol{\Psi}_{\triangle t}^{\mathscr{A}} \circ \boldsymbol{\Psi}_{\triangle t/2}^{\mathscr{B}}.$$

The higher-order time-splitting methods can be found in the literatures [30, 47].

4.5. Discretization of two-dimensional nonlinear Dirac equation

Using time-splitting technique, the variable coefficient equation (3.4) can be split into three equations — i.e.

$$\partial_t \boldsymbol{\Psi}(x_1, x_2, t) = -\boldsymbol{\alpha_1} c_1(x_1)\partial_{x_1}\boldsymbol{\Psi} =: \mathscr{A}_1\boldsymbol{\Psi}(x_1, x_2, t), \quad (x_1, x_2) \in \mathscr{D}, \tag{4.12}$$
$$\partial_t \boldsymbol{\Psi}(x_1, x_2, t) = -\boldsymbol{\alpha_2} c_2(x_2)\partial_{x_2}\boldsymbol{\Psi} =: \mathscr{A}_2\boldsymbol{\Psi}(x_1, x_2, t), \quad (x_1, x_2) \in \mathscr{D}, \tag{4.13}$$
$$\partial_t \boldsymbol{\Psi}(x_1, x_2, t) = -if(\boldsymbol{\Psi}^\dagger\boldsymbol{\beta}\boldsymbol{\Psi})\boldsymbol{\beta}\boldsymbol{\Psi} =: \mathscr{B}\boldsymbol{\Psi}(x_1, x_2, t), \quad (x_1, x_2) \in \mathscr{D}, \tag{4.14}$$

where

$$\boldsymbol{\Psi}(x_1, x_2, t) = \big(\Psi_1(x_1, x_2, t), \Psi_2(x_1, x_2, t), \Psi_3(x_1, x_2, t), \Psi_4(x_1, x_2, t)\big)^T, \quad t \in [0, T],$$

and $\mathscr{D} = (x_{1,L}^*, x_{1,R}^*) \times (x_{2,L}^*, x_{2,R}^*)$ is the computational domain. Note that the operator $\mathscr{A}_1$ is linear in the x_1-direction, the operator $\mathscr{A}_2$ is linear in the x_2-direction, and the operator $\mathscr{B}$ is nonlinear.

Given two even positive integers N_1, N_2, we choose the spatial mesh size $h_1 = (x^*_{1,R} - x^*_{1,L})/N_1$ in the x_1-direction and $h_2 = (x^*_{2,R} - x^*_{2,L})/N_2$ in the x_2-direction. Choose the time step as $\triangle t = T/M$ with a constant M, and consider the grid points

$$\begin{aligned} x_{1,k_1} &= x^*_{1,L} + k_1 h_1, \quad k_1 = 0,1,\ldots,N_1, \\ x_{2,k_2} &= x^*_{2,L} + k_2 h_2, \quad k_2 = 0,1,\ldots,N_2, \\ t_n &= n\triangle t, \qquad\qquad n = 0,1,\ldots,M. \end{aligned}$$

Let

$$\Psi^n_{\eta,k_1,k_2} \approx \Psi_\eta(x_{1,k_1}, x_{2,k_2}, t_n), \quad \eta = 1,\ldots,4,$$

and $\boldsymbol{\Psi}^n_{\boldsymbol{\eta}} = \{\Psi^n_{\eta,k_1,k_2}\}^{N_1-1,N_2-1}_{k_1,k_2=0}$, $\eta = 1,\ldots,4$ be the solution matrix.

Remark 4.3. If we apply the first-order splitting method to solve Eqs. (3.4)-(3.6) in time, the approximate solution $\boldsymbol{\Psi}^I$ can be represented as

$$\boldsymbol{\Psi}^I = \boldsymbol{\Psi}^{\mathscr{B}}_{\triangle t} \circ \boldsymbol{\Psi}^{\mathscr{A}_2}_{\triangle t} \circ \boldsymbol{\Psi}^{\mathscr{A}_1}_{\triangle t},$$

where $\boldsymbol{\Psi}^{\mathscr{A}_1}_{\triangle t}$ is the approximation solution of the linear equation (4.12), $\boldsymbol{\Psi}^{\mathscr{A}_2}_{\triangle t}$ denotes the approximation solution of (4.13) and $\boldsymbol{\Psi}^{\mathscr{B}}_{\triangle t}$ is the exact solution of the nonlinear equation (4.14).

4.6. Fourier-collocation discretization of the linear equation (4.12) in space

Here, we use the FC method to solve the Eq. (4.12) in space. Note that the Dirac matrix $\boldsymbol{\alpha}_1$ can be factorized as $\boldsymbol{\alpha}_1 = \boldsymbol{\Pi}_1 \boldsymbol{\Lambda} \boldsymbol{\Pi}_1^\dagger$ with

$$\boldsymbol{\Lambda} = \begin{pmatrix} 1 & 0 & 0 & 0 \\ 0 & 1 & 0 & 0 \\ 0 & 0 & -1 & 0 \\ 0 & 0 & 0 & -1 \end{pmatrix}, \quad \boldsymbol{\Pi}_1 = 1/\sqrt{2} \begin{pmatrix} 0 & 1 & 1 & 0 \\ 1 & 0 & 0 & -1 \\ 1 & 0 & 0 & 1 \\ 0 & 1 & -1 & 0 \end{pmatrix}, \quad \boldsymbol{\Pi}_1^\dagger = \overline{\boldsymbol{\Pi}}_1^T.$$

Using this matrix factorization gives

$$\begin{aligned} \Phi_1 &= 1/\sqrt{2}\Psi_2 + 1/\sqrt{2}\Psi_3, \quad \Phi_2 = 1/\sqrt{2}\Psi_1 + 1/\sqrt{2}\Psi_4, \\ \Phi_3 &= 1/\sqrt{2}\Psi_1 - 1/\sqrt{2}\Psi_4, \quad \Phi_4 = -1/\sqrt{2}\Psi_2 + 1/\sqrt{2}\Psi_3, \end{aligned}$$

and we arrive at the following decoupled system of PDEs for Φ_1, Φ_2, Φ_3 and Φ_4:

$$\begin{aligned} \partial_t \Phi_1 &= -c_1(x_1)\partial_{x_1}\Phi_1, \quad \partial_t \Phi_2 = -c_1(x_1)\partial_{x_1}\Phi_2, \\ \partial_t \Phi_3 &= c_1(x_1)\partial_{x_1}\Phi_3, \qquad \partial_t \Phi_4 = c_1(x_1)\partial_{x_1}\Phi_4 \end{aligned} \tag{4.15}$$

with unknown functions $\Phi_\eta = \Phi_\eta(x_1, x_2, t)$, $\eta = 1,\ldots,4$.

Consider the following approximations of the functions $\Phi_\eta(x_1,x_2,t)$:

$$\begin{aligned}\Phi_\eta(x_1,x_2,t) &\approx \Phi_{\eta,N_1,N_2}(x_1,x_2,t)\\ &= \sum_{j_1=0}^{N_1-1}\sum_{j_2=0}^{N_2-1}\Phi_{\eta,j_1,j_2}(t)\,L_{j_1}(\overline{x}_1)\,L_{j_2}(\overline{x}_2),\quad \eta=1,\dots,4,\end{aligned}\tag{4.16}$$

where

$$\begin{aligned}\overline{x}_1 &= 2\pi(x_1-x^*_{1,L})/(x^*_{1,R}-x^*_{1,L})\in[0,2\pi],\\ \overline{x}_2 &= 2\pi(x_2-x^*_{2,L})/(x^*_{2,R}-x^*_{2,L})\in[0,2\pi].\end{aligned}$$

Substituting (4.16) into (4.15) and collocating the results at the grid points $(x_1,x_2)=(x_{1,k_1},x_{2,k_2})$, for every $k_1=0,1,\dots,N_1-1$, $k_2=0,1,\dots,N_2-1$, we obtain the discrete system of ordinary differential equations

$$\begin{aligned}\partial_t\Phi_{1,k_1,k_2}(t) &= -\gamma_1 c(x_{1,k_1})\sum_{j_1=0}^{N_1-1} d_{k_1,j_1}\Phi_{1,j_1,k_2}(t),\\ \partial_t\Phi_{2,k_1,k_2}(t) &= -\gamma_1 c(x_{1,k_1})\sum_{j_1=0}^{N_1-1} d_{k_1,j_1}\Phi_{2,j_1,k_2}(t),\\ \partial_t\Phi_{3,k_1,k_2}(t) &= \gamma_1 c(x_{1,k_1})\sum_{j_1=0}^{N_1-1} d_{k_1,j_1}\Phi_{3,j_1,k_2}(t),\\ \partial_t\Phi_{4,k_1,k_2}(t) &= \gamma_1 c(x_{1,k_1})\sum_{j_1=0}^{N_1-1} d_{k_1,j_1}\Phi_{4,j_1,k_2}(t)\end{aligned}$$

with $\gamma_1=2\pi/(x^*_{1,R}-x^*_{1,L})$. This system can be written in the matrix form as

$$\begin{aligned}&\partial_t\boldsymbol{\Phi_1}=-\gamma_1\boldsymbol{G_1}\boldsymbol{\Phi_1},\quad \partial_t\boldsymbol{\Phi_2}=-\gamma_1\boldsymbol{G_1}\boldsymbol{\Phi_2},\\ &\partial_t\boldsymbol{\Phi_3}=\gamma_1\boldsymbol{G_1}\boldsymbol{\Phi_3},\qquad \partial_t\boldsymbol{\Phi_4}=\gamma_1\boldsymbol{G_1}\boldsymbol{\Phi_4},\end{aligned}\tag{4.17}$$

where $\boldsymbol{\Phi_\eta}=\boldsymbol{\Phi_\eta}(t)=\{\Phi_{\eta,k_1,k_2}(t)\}_{k_1,k_2=0}^{N_1-1,N_2-1}$, $\eta=1,2,3,4$ is the unknown matrix and $\boldsymbol{G_1}=\boldsymbol{C_1}\boldsymbol{D_1}$ is $N_1\times N_1$ coefficient matrix such that

$$\boldsymbol{C_1}=\operatorname{diag}\big(c_1(x_{1,0}),c_1(x_{1,1}),\dots,c_1(x_{1,N_1-1})\big),\quad \boldsymbol{D_1}=\big\{d_{k_1,j_1}\big\}_{k_1,j_1=0}^{N_1-1}.$$

Similar to one-dimensional NLD equation with PML, the $N_1\times N_1$ matrix $\boldsymbol{G_1}$ can be factorized as $\boldsymbol{P_1}\boldsymbol{\lambda_1}\boldsymbol{P_1^{-1}}$, where $\boldsymbol{\lambda_1}$ and $\boldsymbol{P_1}$ are diagonal and invertible matrices, respectively. We set

$$\begin{pmatrix}\boldsymbol{\phi_1}\\ \boldsymbol{\phi_2}\\ \boldsymbol{\phi_3}\\ \boldsymbol{\phi_4}\end{pmatrix}=\begin{pmatrix}\boldsymbol{P_1^{-1}}\boldsymbol{\Phi_1}\\ \boldsymbol{P_1^{-1}}\boldsymbol{\Phi_2}\\ \boldsymbol{P_1^{-1}}\boldsymbol{\Phi_3}\\ \boldsymbol{P_1^{-1}}\boldsymbol{\Phi_4}\end{pmatrix},$$

and rewrite Eq. (4.17) as

$$\partial_t \boldsymbol{\phi_1} = -\gamma_1 \boldsymbol{\lambda}_1 \boldsymbol{\phi_1}, \quad \partial_t \boldsymbol{\phi_2} = -\gamma_1 \boldsymbol{\lambda}_1 \boldsymbol{\phi_2},$$
$$\partial_t \boldsymbol{\phi_3} = \gamma_1 \boldsymbol{\lambda}_1 \boldsymbol{\phi_3}, \quad \partial_t \boldsymbol{\phi_4} = \gamma_1 \boldsymbol{\lambda}_1 \boldsymbol{\phi_4}$$

with unknown matrix $\boldsymbol{\phi_\eta} = \boldsymbol{\phi_\eta}(t) = \{\phi_{\eta,k_1,k_2}(t)\}_{k_1,k_2=0}^{N_1-1,N_2-1}$, $\eta = 1,2,3,4$. The latter system can be also written as

$$\begin{aligned}
\partial_t \phi_{1,k_1,k_2} &= -\gamma_1 \lambda_{1,k_1} \phi_{1,k_1,k_2}, \\
\partial_t \phi_{2,k_1,k_2} &= -\gamma_1 \lambda_{1,k_1} \phi_{2,k_1,k_2}, \\
\partial_t \phi_{3,k_1,k_2} &= \gamma_1 \lambda_{1,k_1} \phi_{3,k_1,k_2}, \\
\partial_t \phi_{4,k_1,k_2} &= \gamma_1 \lambda_{1,k_1} \phi_{4,k_1,k_2},
\end{aligned} \tag{4.18}$$

where $\boldsymbol{\lambda}_1 = \mathrm{diag}(\lambda_{1,0}, \lambda_{1,1}, \ldots, \lambda_{1,N_1-1})$. For any k_1, k_2, the exact solution of the Eq. (4.18) over $[t_n, t_{n+1}]$ has the form

$$\begin{aligned}
\phi_{1,k_1,k_2}^{n+1} &= e^{-\gamma_1 \lambda_{1,k_1} \triangle t} \phi_{1,k_1,k_2}^{n}, \\
\phi_{2,k_1,k_2}^{n+1} &= e^{-\gamma_1 \lambda_{1,k_1} \triangle t} \phi_{2,k_1,k_2}^{n}, \\
\phi_{3,k_1,k_2}^{n+1} &= e^{\gamma_1 \lambda_{1,k_1} \triangle t} \phi_{3,k_1,k_2}^{n}, \\
\phi_{4,k_1,k_2}^{n+1} &= e^{\gamma_1 \lambda_{1,k_1} \triangle t} \phi_{4,k_1,k_2}^{n}.
\end{aligned}$$

Consequently, using the matrix $\boldsymbol{\phi}_{\boldsymbol{\eta}}^{n+1} = \{\phi_{\eta,k_1,k_2}^{n+1}\}_{k_1,k_2=0}^{N_1-1,N_2-1}$, $\eta = 1,2,3,4$, we can derive the following numerical solutions of the system (4.12):

$$\begin{aligned}
\boldsymbol{\Psi_1}^{n+1} &= 1/\sqrt{2}\boldsymbol{P_1}\boldsymbol{\phi_2}^{n+1} + 1/\sqrt{2}\boldsymbol{P_1}\boldsymbol{\phi_3}^{n+1}, \\
\boldsymbol{\Psi_2}^{n+1} &= 1/\sqrt{2}\boldsymbol{P_1}\boldsymbol{\phi_1}^{n+1} - 1/\sqrt{2}\boldsymbol{P_1}\boldsymbol{\phi_4}^{n+1}, \\
\boldsymbol{\Psi_3}^{n+1} &= 1/\sqrt{2}\boldsymbol{P_1}\boldsymbol{\phi_1}^{n+1} + 1/\sqrt{2}\boldsymbol{P_1}\boldsymbol{\phi_4}^{n+1}, \\
\boldsymbol{\Psi_4}^{n+1} &= 1/\sqrt{2}\boldsymbol{P_1}\boldsymbol{\phi_2}^{n+1} - 1/\sqrt{2}\boldsymbol{P_1}\boldsymbol{\phi_3}^{n+1},
\end{aligned}$$

where $\boldsymbol{\Psi}_{\boldsymbol{\eta}}^{n+1} = \{\Psi_{\eta,k_1,k_2}^{n+1}\}_{k_1,k_2=0}^{N_1-1,N_2-1}$, $\eta = 1,2,3,4$.

4.7. Fourier-collocation discretization for the linear part (4.13) in space

In the following, we apply the FC method to solve Eq. (4.13) in space. The Dirac matrix $\boldsymbol{\alpha}_2$ is factorized as $\boldsymbol{\Pi}_2 \boldsymbol{\Lambda} \boldsymbol{\Pi}_2^{\dagger}$ with the matrices

$$\boldsymbol{\Pi}_2 = 1/\sqrt{2}\begin{pmatrix} 0 & -i & -i & 0 \\ 1 & 0 & 0 & 1 \\ -i & 0 & 0 & i \\ 0 & 1 & -1 & 0 \end{pmatrix}, \quad \boldsymbol{\Pi}_2^{\dagger} = 1/\sqrt{2}\begin{pmatrix} 0 & 1 & i & 0 \\ i & 0 & 0 & 1 \\ i & 0 & 0 & -1 \\ 0 & 1 & -i & 0 \end{pmatrix},$$

and the diagonal matrix $\boldsymbol{\Lambda} = \mathrm{diag}(1,1,-1,-1)$. Therefore, introducing the functions

$$\Phi_1 = 1/\sqrt{2}\Psi_2 + i/\sqrt{2}\Psi_3, \quad \Phi_2 = i/\sqrt{2}\Psi_1 + 1/\sqrt{2}\Psi_4,$$
$$\Phi_3 = i/\sqrt{2}\Psi_2 - 1/\sqrt{2}\Psi_4, \quad \Phi_4 = 1/\sqrt{2}\Psi_2 - i/\sqrt{2}\Psi_3,$$

we rewrite the Eq. (4.13) as

$$\begin{aligned} &\partial_t \Phi_1 = -c_2(x_2)\partial_{x_2}\Phi_1, \quad \partial_t \Phi_2 = -c_2(x_2)\partial_{x_2}\Phi_2, \\ &\partial_t \Phi_3 = c_2(x_2)\partial_{x_2}\Phi_3, \qquad \partial_t \Phi_4 = c_2(x_2)\partial_{x_2}\Phi_4 \end{aligned} \tag{4.19}$$

with unknown functions $\Phi_\eta = \Phi_\eta(x_1, x_2, t)$, $\eta = 1, 2, 3, 4$.

Similar to two-dimensional NLD equation with PML in the x_1-direction (4.12), we substitute (4.16) into (4.19) and solve the resulting equations one by one by applying the matrix factorization technique. Finally, we get the approximate solution of (4.13) over $[t_n, t_{n+1}]$.

4.8. Exact solution of nonlinear equation (4.14)

Taking into account the relations

$$\begin{aligned} &\partial_t \boldsymbol{\Psi}(x_1, x_2, t) = -if\big(|\Psi_1|^2 + |\Psi_2|^2 - |\Psi_3|^2 - |\Psi_4|^2\big)\boldsymbol{\beta}\boldsymbol{\Psi}(x_1, x_2, t), \quad t \in [t_n, t_{n+1}], \\ &\partial_t \overline{\boldsymbol{\Psi}}(x_1, x_2, t) = if\big(|\Psi_1|^2 + |\Psi_2|^2 - |\Psi_3|^2 - |\Psi_4|^2\big)\boldsymbol{\beta}\overline{\boldsymbol{\Psi}}(x_1, x_2, t), \qquad t \in [t_n, t_{n+1}], \end{aligned}$$

we get

$$\partial_t |\boldsymbol{\Psi}(x_1, x_2, t)|^2 = \partial_t\big(\boldsymbol{\Psi}(x_1, x_2, t)\overline{\boldsymbol{\Psi}}(x_1, x_2, t)\big) = \mathbf{0}, \quad t \in [t_n, t_{n+1}].$$

Therefore,

$$|\boldsymbol{\Psi}(x_1, x_2, t)|^2 = |\boldsymbol{\Psi}(x_1, x_2, t_n)|^2, \quad t \in [t_n, t_{n+1}]$$

and we only have to solve the following ODEs:

$$\partial_t \boldsymbol{\Psi}(x_1, x_2, t) = -if(x_1, x_2, t_n)\boldsymbol{\beta}\boldsymbol{\Psi}(x_1, x_2, t), \quad t \in [t_n, t_{n+1}], \tag{4.20}$$

where

$$f(x_1, x_2, t_n) = f\big(|\Psi_1(x_1, x_2, t_n)|^2 + |\Psi_2(x_1, x_2, t_n)|^2 - |\Psi_3(x_1, x_2, t_n)|^2 - |\Psi_4(x_1, x_2, t_n)|^2\big).$$

Setting $f^n_{k_1,k_2} \approx f(x_{1,k_1}, x_{2,k_2}, t_n)$, we determine the exact solution of (4.20) over $[t_n, t_{n+1}]$, so that

$$\begin{aligned} &\Psi^{n+1}_{1,k_1,k_2} = e^{-if^n_{k_1,k_2}\triangle t}\Psi^n_{1,k_1,k_2}, \quad \Psi^{n+1}_{2,k_1,k_2} = e^{-if^n_{k_1,k_2}\triangle t}\Psi^n_{2,k_1,k_2}, \\ &\Psi^{n+1}_{3,k_1,k_2} = e^{if^n_{k_1,k_2}\triangle t}\Psi^n_{3,k_1,k_2}, \quad \Psi^{n+1}_{4,k_1,k_2} = e^{if^n_{k_1,k_2}\triangle t}\Psi^n_{4,k_1,k_2} \end{aligned}$$

for every k_1, k_2.

Finally, the TSFC method to solve two-dimensional Eq. (3.4) is summarized in Algorithm 4.2.

Algorithm 4.2 Time-Splitting Fourier-Collocation Method for 2D System (3.4)

1: Given initial values $\boldsymbol{\Psi}^0_\eta = \{\Psi_\eta(x_1, x_2, 0)\}^{N_1-1,N_2-1}_{k_1,k_2=0}, \eta = 1, \ldots, 4$.
2: $M = T/\triangle t$, $\triangle t$ is the time step.
3: Let the Dirac matrix $\boldsymbol{\alpha}_1 = \boldsymbol{\Pi}_1\boldsymbol{\Lambda}\boldsymbol{\Pi}_1^\dagger$ and $\boldsymbol{\alpha}_2 = \boldsymbol{\Pi}_2\boldsymbol{\Lambda}\boldsymbol{\Pi}_2^\dagger$.

4: Find coefficient matrix $\boldsymbol{G_1} = \boldsymbol{P_1}\boldsymbol{\lambda_1}\boldsymbol{P_1^{-1}}$ in the x_1-direction with

$$\boldsymbol{\lambda_1} = \mathrm{diag}(\lambda_{1,0}, \lambda_{1,1}, \ldots, \lambda_{1,N_1-1}),$$

and $\boldsymbol{G_2} = \boldsymbol{P_2}\boldsymbol{\lambda_2}\boldsymbol{P_2^{-1}}$ in the x_2-direction with

$$\boldsymbol{\lambda_2} = \mathrm{diag}(\lambda_{2,0}, \lambda_{2,1}, \ldots, \lambda_{2,N_1-1}).$$

5: **for** $n = 0 : M-1$ **do**

6: Get

$$\begin{aligned} \boldsymbol{\Phi_1^n} &= 1/\sqrt{2}\boldsymbol{\Psi_2^n} + 1/\sqrt{2}\boldsymbol{\Psi_3^n}, \quad \boldsymbol{\Phi_2^n} = 1/\sqrt{2}\boldsymbol{\Psi_1^n} + 1/\sqrt{2}\boldsymbol{\Psi_4^n}, \\ \boldsymbol{\Phi_3^n} &= 1/\sqrt{2}\boldsymbol{\Psi_1^n} - 1/\sqrt{2}\boldsymbol{\Psi_4^n}, \quad \boldsymbol{\Phi_4^n} = -1/\sqrt{2}\boldsymbol{\Psi_2^n} + 1/\sqrt{2}\boldsymbol{\Psi_3^n}. \end{aligned}$$

7: Calculate

$$\begin{aligned} \boldsymbol{\Phi_1^*} &= \boldsymbol{P_1} e^{-\gamma_1 \boldsymbol{\lambda_1} \triangle t} \boldsymbol{P_1^{-1}} \boldsymbol{\Phi_1^n}, \quad \boldsymbol{\Phi_2^*} = \boldsymbol{P_1} e^{-\gamma_1 \boldsymbol{\lambda_1} \triangle t} \boldsymbol{P_1^{-1}} \boldsymbol{\Phi_2^n}, \\ \boldsymbol{\Phi_3^*} &= \boldsymbol{P_1} e^{\gamma_1 \boldsymbol{\lambda_1} \triangle t} \boldsymbol{P_1^{-1}} \boldsymbol{\Phi_3^n}, \quad \boldsymbol{\Phi_4^*} = \boldsymbol{P_1} e^{\gamma_1 \boldsymbol{\lambda_1} \triangle t} \boldsymbol{P_1^{-1}} \boldsymbol{\Phi_4^n}. \end{aligned}$$

8: Compute

$$\begin{aligned} \boldsymbol{\Psi_1^*} &= 1/\sqrt{2}\boldsymbol{\Phi_2^*} + 1/\sqrt{2}\boldsymbol{\Phi_3^*}, \quad \boldsymbol{\Psi_2^*} = 1/\sqrt{2}\boldsymbol{\Phi_1^*} - 1/\sqrt{2}\boldsymbol{\Phi_4^*}, \\ \boldsymbol{\Psi_3^*} &= 1/\sqrt{2}\boldsymbol{\Phi_1^*} + 1/\sqrt{2}\boldsymbol{\Phi_4^*}, \quad \boldsymbol{\Psi_4^*} = 1/\sqrt{2}\boldsymbol{\Phi_2^*} - 1/\sqrt{2}\boldsymbol{\Phi_3^*}. \end{aligned}$$

9: Require $\widetilde{\boldsymbol{\Psi_\eta^*}} = (\boldsymbol{\Psi_\eta^*})^T$, $\eta = 1, 2, 3, 4$,

$$\begin{aligned} \widetilde{\boldsymbol{\Phi_1^*}} &= 1/\sqrt{2}\widetilde{\boldsymbol{\Psi_2^*}} + i/\sqrt{2}\widetilde{\boldsymbol{\Psi_3^*}}, \quad \widetilde{\boldsymbol{\Phi_2^*}} = i/\sqrt{2}\widetilde{\boldsymbol{\Psi_1^*}} + 1/\sqrt{2}\widetilde{\boldsymbol{\Psi_4^*}}, \\ \widetilde{\boldsymbol{\Phi_3^*}} &= i/\sqrt{2}\widetilde{\boldsymbol{\Psi_1^*}} - 1/\sqrt{2}\widetilde{\boldsymbol{\Psi_4^*}}, \quad \widetilde{\boldsymbol{\Phi_4^*}} = 1/\sqrt{2}\widetilde{\boldsymbol{\Psi_2^*}} - i/\sqrt{2}\widetilde{\boldsymbol{\Psi_3^*}}. \end{aligned}$$

10: Calculate

$$\begin{aligned} \boldsymbol{\Phi_1^{**}} &= \boldsymbol{P_2} e^{-\gamma_2 \boldsymbol{\lambda_2} \triangle t} \boldsymbol{P_2^{-1}} \widetilde{\boldsymbol{\Phi_1^*}}, \quad \boldsymbol{\Phi_2^{**}} = \boldsymbol{P_2} e^{-\gamma_2 \boldsymbol{\lambda_2} \triangle t} \boldsymbol{P_2^{-1}} \widetilde{\boldsymbol{\Phi_2^*}}, \\ \boldsymbol{\Phi_3^{**}} &= \boldsymbol{P_2} e^{\gamma_2 \boldsymbol{\lambda_2} \triangle t} \boldsymbol{P_2^{-1}} \widetilde{\boldsymbol{\Phi_3^*}}, \quad \boldsymbol{\Phi_4^{**}} = \boldsymbol{P_2} e^{\gamma_2 \boldsymbol{\lambda_2} \triangle t} \boldsymbol{P_2^{-1}} \widetilde{\boldsymbol{\Phi_4^*}}. \end{aligned}$$

11: Calculate

$$\begin{aligned} \widetilde{\boldsymbol{\Psi_1^{**}}} &= -i/\sqrt{2}\boldsymbol{\Phi_2^{**}} - i/\sqrt{2}\boldsymbol{\Phi_3^{**}}, \quad \widetilde{\boldsymbol{\Psi_2^{**}}} = 1/\sqrt{2}\boldsymbol{\Phi_1^{**}} + 1/\sqrt{2}\boldsymbol{\Phi_4^{**}}, \\ \widetilde{\boldsymbol{\Psi_3^{**}}} &= -i/\sqrt{2}\boldsymbol{\Phi_1^{**}} + i/\sqrt{2}\boldsymbol{\Phi_4^{**}}, \quad \widetilde{\boldsymbol{\Psi_4^{**}}} = 1/\sqrt{2}\boldsymbol{\Phi_2^{**}} - 1/\sqrt{2}\boldsymbol{\Phi_3^{**}}. \end{aligned}$$

12: Set $\boldsymbol{\Psi_\eta^{**}} = (\widetilde{\boldsymbol{\Psi_\eta^{**}}})^T$, $\eta = 1, 2, 3, 4$, $\boldsymbol{f^{**}} = f(|\boldsymbol{\Psi_1^{**}}|^2 + |\boldsymbol{\Psi_2^{**}}|^2 - |\boldsymbol{\Psi_3^{**}}|^2 - |\boldsymbol{\Psi_4^{**}}|^2)$.

13: Obtain $\boldsymbol{\Psi_1^{n+1}}$, $\boldsymbol{\Psi_2^{n+1}}$, $\boldsymbol{\Psi_3^{n+1}}$ and $\boldsymbol{\Psi_4^{n+1}}$ from

$$\begin{aligned} \Psi^{n+1}_{1,k_1,k_2} &= e^{-if^{**}_{k_1,k_2}\triangle t}\Psi^{**}_{1,k_1,k_2}, \quad \Psi^{n+1}_{2,k_1,k_2} = e^{-if^{**}_{k_1,k_2}\triangle t}\Psi^{**}_{2,k_1,k_2}, \\ \Psi^{n+1}_{3,k_1,k_2} &= e^{if^{**}_{k_1,k_2}\triangle t}\Psi^{**}_{3,k_1,k_2}, \quad \Psi^{n+1}_{4,k_1,k_2} = e^{if^{**}_{k_1,k_2}\triangle t}\Psi^{**}_{4,k_1,k_2}, \end{aligned}$$

$k_1 = 0, 1, \ldots, N_1 - 1, k_2 = 0, 1, \ldots, N_2 - 1$.

14: **end for**

5. Numerical Results

Note that the following absorption functions $\sigma(x)$ have been well studied and successfully applied for Dirac equation [7,8]:

$$\begin{array}{llll} \text{Type I:} & \sigma_0(x_j+\delta_j)^2, & \text{Type II:} & \sigma_0(x_j+\delta_j)^3, \\ \text{Type III:} & -\sigma_0/x_j, & \text{Type IV:} & \sigma_0/x_j^2, \\ \text{Type V:} & -\sigma_0/x_j-\sigma_0/\delta_j, & \text{Type VI:} & \sigma_0/x_j^2-\sigma_0/\delta_j^2, \end{array}$$

where $\sigma_0>0$ is the absorption strength, δ_j the thickness of the layer, $j=1,\ldots,d$, and d is the dimension. We use Type I absorption function in all examples, and in tests we choose the same coefficients $\sigma_0=$ 1e-03 and $\theta=\pi/4$ for all layers in different directions.

We use $E_{\Psi_l}(t)$ to denote the error measure,

$$E_{\Psi_l}(t)=\left\|\Psi_l^{exact}(\cdot,t)-\Psi_l^{\boldsymbol{h},\triangle t}(\cdot,t)\right\|_\infty.$$

In one-dimensional case, $l=1,2$, and two-dimensional case $l=1,2,3,4$. Besides, $\Psi_l^{exact}(\cdot,t)$ is the l-component exact solution of the equation, $\Psi_l^{\boldsymbol{h},\triangle t}$ is the l-component numerical solution obtained by the TSFC method or the TSFS method [8] with the mesh size $\boldsymbol{h}=(h_1,\ldots,h_d)$ $(d=1,2)$ and time step $\triangle t$.

5.1. Numerical results in one dimension

In this section, we choose two different initial conditions to study the behavior of the TSFC scheme proposed in Sections 4.2-4.4 for solving Eqs. (3.1)-(3.3).

Firstly, we take initial conditions as

$$\Psi_1(x_1,t=0)=\Psi_2(x_1,t=0)=e^{i3x_1}e^{-x_1^2}$$

in Table 1-2. We present the spatial-temporal error analysis for the TSFC method and TSFS method, respectively. We assume the numerical solution with fine mesh size — viz. $h_1=1/16,\triangle t=$1e-03, is the exact solution. These solution is denoted by $\Psi_1^{exact},\Psi_2^{exact}$. Table 1 shows that the proposed TSFC method has spectral convergence in space, but the TSFS method does not. In the latter method, the decrease of spatial size does not necessarily

Table 1: Spatial error analysis of two numerical methods to 1D NLD equation with PML, $x_1\in\overline{\mathscr{D}}=[-4-\delta,4+\delta]$, $\delta=1$.

	TSFS			TSFC		
Error	$h_1=1/2$	$h_1=1/4$	$h_1=1/8$	$h_1=1/2$	$h_1=1/4$	$h_1=1/8$
$E_{\Psi_1}(t=2)$	1.0482e-01	2.5363e-03	1.6087e-03	6.7865e-02	3.1890e-04	1.0978e-08
$E_{\Psi_2}(t=2)$	7.4923e-02	2.5516e-03	1.6571e-03	3.7200e-02	3.3529e-04	1.1648e-08
CPU time(s)	0.056260	0.086483	0.122132	0.130181	0.300863	1.109481

Table 2: Temporal error analysis of two numerical methods to 1D NLD equation with PML, $x_1 \in \overline{\mathscr{D}} = [-4-\delta, 4+\delta]$, $\delta = 1$.

	TSFS			TSFC		
Error	$8\triangle t$	$4\triangle t$	$2\triangle t$	$8\triangle t$	$4\triangle t$	$2\triangle t$
$E_{\Psi_1}(t=2)$	7.7024e-02	3.3488e-02	1.0734e-02	3.0060e-03	1.2884e-03	4.2949e-04
$E_{\Psi_2}(t=2)$	7.3025e-02	3.1576e-02	9.6503e-03	3.0084e-03	1.2890e-03	4.2960e-04
CPU time(s)	0.041239	0.059873	0.103965	0.423143	0.776008	1.595562

improve the error. Table 2 demonstrates that although both methods have the first-order numerical error in time, the TSFC method converges faster.

Next, we consider the one-dimensional NLD equation (2.6) with the exact solution

$$\Psi_1^{exact}(x_1,t) = \left(\frac{\sqrt{(\gamma+1)(1-\Lambda^2)(1+\Lambda)}\cosh(\sqrt{1-\Lambda^2}\gamma(x_1-\nu t))}{1+\Lambda\cosh(2\sqrt{1-\Lambda^2}\gamma(x_1-\nu t))} \right.$$
$$\left. +\text{sign}(\nu)\frac{i\sqrt{(\gamma-1)(1-\Lambda^2)(1-\Lambda)}\sinh(\sqrt{1-\Lambda^2}\gamma(x_1-\nu t))}{1+\Lambda\cosh(2\sqrt{1-\Lambda^2}\gamma(x_1-\nu t))} \right) e^{-i\Lambda\gamma(t-\nu x_1)},$$

$$\Psi_2^{exact}(x_1,t) = \left(\frac{i\sqrt{(\gamma+1)(1-\Lambda^2)(1-\Lambda)}\sinh(\sqrt{1-\Lambda^2}\gamma(x_1-\nu t))}{1+\Lambda\cosh(2\sqrt{1-\Lambda^2}\gamma(x_1-\nu t))} \right.$$
$$\left. +\text{sign}(\nu)\frac{\sqrt{(\gamma-1)(1-\Lambda^2)(1+\Lambda)}\cosh(\sqrt{1-\Lambda^2}\gamma(x_1-\nu t))}{1+\Lambda\cosh(2\sqrt{1-\Lambda^2}\gamma(x_1-\nu t))} \right) e^{-i\Lambda\gamma(t-\nu x_1)}$$

with $\Lambda = 0.75, \gamma = 1/\sqrt{1-\nu^2}$ and $\nu \in \mathbb{R}$. We choose the following initial conditions for one-dimensional system (3.1)-(3.3):

$$\Psi_1(x_1,t=0) = \Psi_1^{exact}(x_1,t=0), \quad \Psi_2(x_1,t=0) = \Psi_2^{exact}(x_1,t=0). \tag{5.1}$$

Figs. 3-4 demonstrate interaction dynamics — e.g. the movement of a single traveling solitary wave and the collision of multiple Dirac solitary waves on the domain $\overline{\mathscr{D}} = [-8-\delta_1, 8+\delta_1]$, $\delta_1 = 3$. Fig. 3 reflects different choice of ν in the initial condition (5.1) and shows the absolute value function $|\Psi_1(x_1,t)|$ at different time. Note that if $\nu < 0$, the wave travels from right to left, and no boundary reflections are observed due to the PML. If $\nu > 0$, the wave propagates from left to right, and the numerical results again show no boundary reflections.

In Fig. 4, we display the results in the case of the initial conditions

$$\Psi_1(x_1,t=0) = \Psi_1^{exact}(x_1+5,t=0) + \Psi_1^{exact}(x_1-5,t=0),$$
$$\Psi_2(x_1,t=0) = \Psi_2^{exact}(x_1+5,t=0) + \Psi_2^{exact}(x_1-5,t=0).$$

In the simulation, the collision of two Dirac solitary waves has been shown. After $t = 15$, the numerical solution obtained without PML is reflected at the boundaries, while solutions obtained with PML can avoid boundary reflections at a large time.

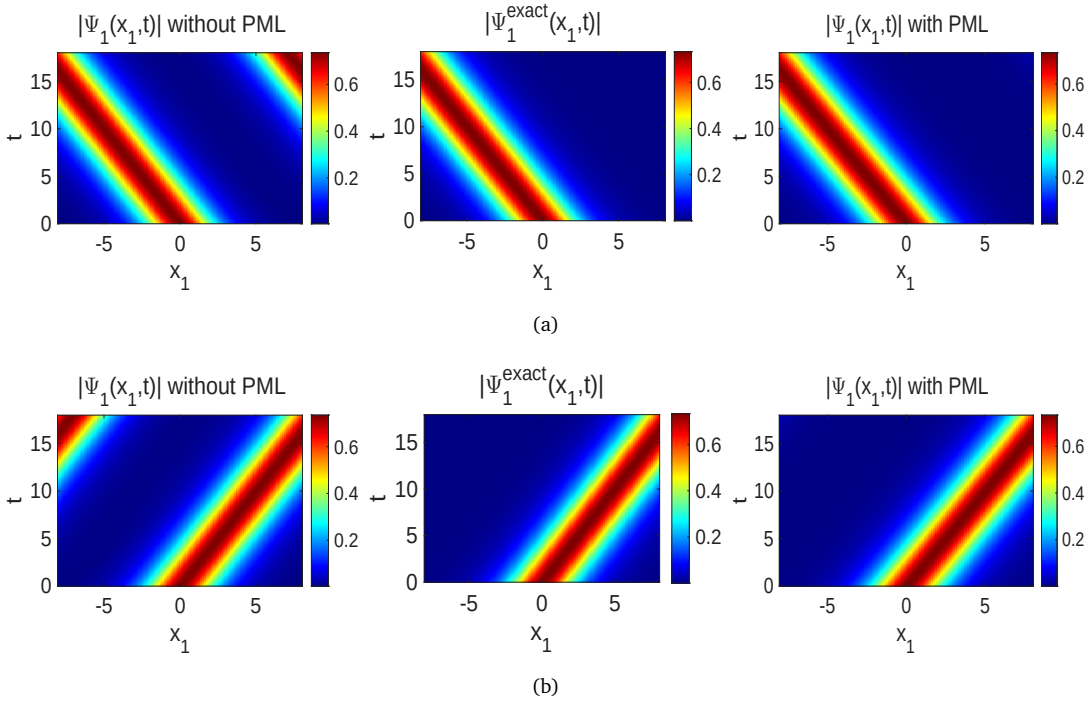

Figure 3: Time evolution of $|\Psi_1(x_1,t)|$. Left: Solution without PML. Middle: Exact solution. Right: Solution with PML. (a) Wave function travels from right to left, $v=-0.5$. (b) Wave function travels from left to right, $v=0.5$.

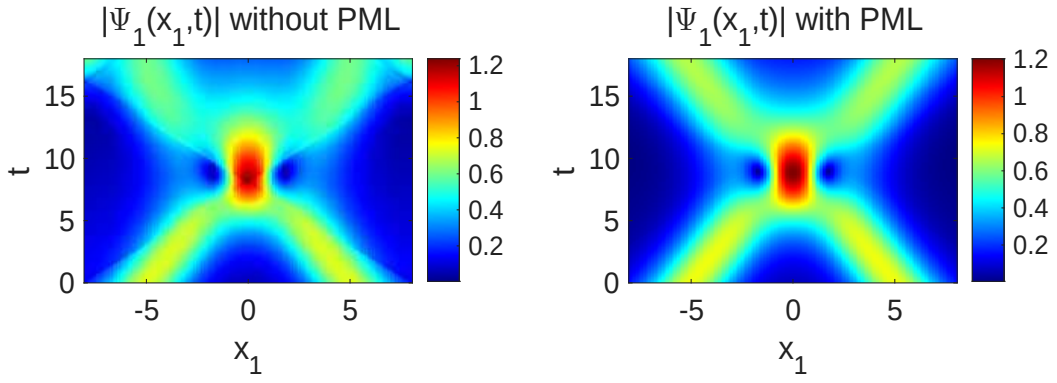

Figure 4: Simulation of collision of two traveling solitons: solution without PML (left) and solution with PML (right).

5.2. Numerical tests in two dimension

Consider the two-dimensional NLD equation with PML (3.4)-(3.6) with the Gaussian-like initial conditions

$$\Psi_l(x_1,x_2,t=0)=e^{i3x_1}e^{-(x_1^2+x_2^2)},\quad l=1,\ldots,4$$

and apply the TSFC method of Sections 4.5-4.8 on the domain $\overline{\mathscr{D}}=[-3-\delta,3+\delta]^2$, $\delta=1$.

Tables 3 and 4 demonstrate spatial-temporal errors of TSFC and TSFS methods. We let Ψ_l^{exact}, $l = 1,2,3,4$, obtained by a numerical method with a very fine mesh and time step — viz. $h_1 = h_2 = h = 1/16$, $\triangle t$ =1e-03, be exact solution. Note that the TSFC method shows better convergence rate in space.

Fig. 5 shows the absorption capability of PML. In the computation, we define the exact solution as $\Psi_1^{EXACT}(x_1, x_2, t)$ which is obtained with a fine mesh on domain $[-15, 15]^2$. With the time evolution of the function $|\Psi_1(x_1, 0, t)|$, we find that the numerical solution obtained without PML is reflected at the boundaries when time $t > 1.5$, while the solution with PML can absorb the boundary reflections.

Table 3: Spatial error analysis of two numerical methods for two-dimensional NLD equation with PML.

	TSFS			TSFC		
Error	h=1/2	h=1/4	h=1/8	h=1/2	h=1/4	h=1/8
$E_{\Psi_1}(t=3)$	9.9859e-02	3.0511e-03	1.8773e-03	1.4348e-02	3.4481e-06	7.2895e-07
$E_{\Psi_2}(t=3)$	1.0057e-01	3.0511e-03	1.8773e-03	1.4348e-02	3.4481e-06	7.2895e-07
$E_{\Psi_3}(t=3)$	7.0462e-02	2.9421e-03	1.8796e-03	1.5272e-02	3.3986e-06	7.1236e-07
$E_{\Psi_4}(t=3)$	7.1536e-02	2.9422e-03	1.8796e-03	1.5272e-02	3.3986e-06	7.1236e-07
CPU time(s)	2.280472	6.119786	20.009574	2.040567	6.63113	19.830190

Table 4: Temporal error analysis of two numerical methods for two-dimensional NLD equation with PML.

	TSFS			TSFC		
Error	$8\triangle t$	$4\triangle t$	$2\triangle t$	$8\triangle t$	$4\triangle t$	$2\triangle t$
$E_{\Psi_1}(t=3)$	9.3030e-02	4.1991e-02	1.4375e-02	2.0165e-03	8.7196e-04	2.9195e-04
$E_{\Psi_2}(t=3)$	9.3030e-02	4.1991e-02	1.4375e-02	2.0165e-03	8.7196e-04	2.9195e-04
$E_{\Psi_3}(t=3)$	8.8677e-02	4.0476e-02	1.3936e-02	2.2443e-03	9.6881e-04	3.2412e-04
$E_{\Psi_4}(t=3)$	8.8677e-02	4.0476e-02	1.3936e-02	2.2443e-03	9.6881e-04	3.2412e-04
CPU time(s)	9.494281	19.120353	37.701974	8.852391	17.372556	35.140449

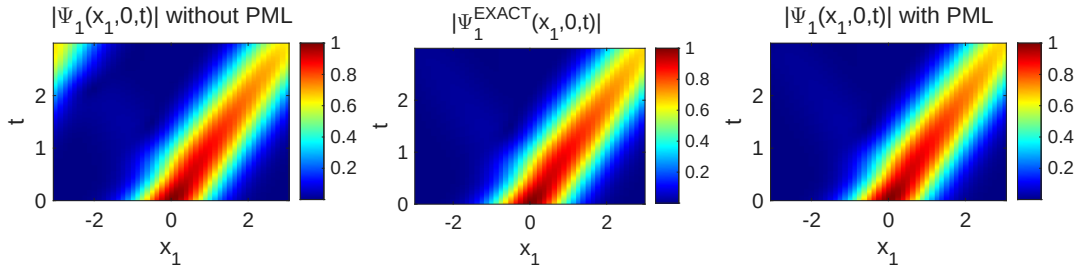

Figure 5: Time evolution of the function $|\Psi_1(x_1, 0, t)|$: solution without PML (left), exact solution (middle) and solution with PML (right).

5.3. Simulation of conical diffraction

Conical diffraction originally arises in nonlinear Schrödinger equation (NLSE) with honeycomb lattice potentials [3, 34]. In the tight-binding limit, one can obtain the evolution equations for the envelopes of two sublattice Bloch modes near the diabolical points. In other words, a Dirac equation is derived directly from the NLSE with the honeycomb lattice. Here, such Dirac equations are used for simulation of the conical diffraction phenomena [3, 34],

$$\partial_t \mathbf{\Phi} = \left(-\boldsymbol{\sigma}_2 \partial_{x_1} + \boldsymbol{\sigma}_1 \partial_{x_2}\right)\mathbf{\Phi} + i(\mathbf{\Phi}^\dagger \mathbf{\Phi})\boldsymbol{I}\mathbf{\Phi},$$

where

$$\mathbf{\Phi} = \mathbf{\Phi}(x_1, x_2, t) = \left(\Phi_1(x_1, x_2, t), \Phi_2(x_1, x_2, t)\right)^T, \quad (x_1, x_2) \in \mathbb{R}^2$$

is unknown wave function. With the dimension reduction of the NLD equation and the proper assumptions on the initial data, we consider a simplified representation of the two-dimensional NLD equation on the x_1x_2-coordinates directly [19, 44], i.e. $\mathbf{\Phi} = (\Psi_1, \Psi_4)^T$ (or $\mathbf{\Phi} = (\Psi_2, \Psi_3)^T$).

In the numerical simulation, we choose the following two sets of initial conditions:

Case A. $\Phi_1(x_1, x_2, t = 0) = e^{-2(x_1^2 + x_2^2)}, \quad \Phi_2(x_1, x_2, t = 0) = 0.$

Cbse B. $\Phi_1(x_1, x_2, t = 0) = \Phi_2(x_1, x_2, t = 0) = e^{-2(x_1^2 + x_2^2)}.$

In Fig. 6, initially, $\Phi_1(x_1, x_2, t)$ is a Gaussian and $\Phi_2(x_1, x_2, t)$ is zero – i.e. Case A. Fig. 6 shows that an initial bell-shaped structure transforms into a ring structure after some distance. The ring structures contain two bright rings, and the outer ring is higher than the inner one. In particular, Poggendorff's dark ring exists between the two bright

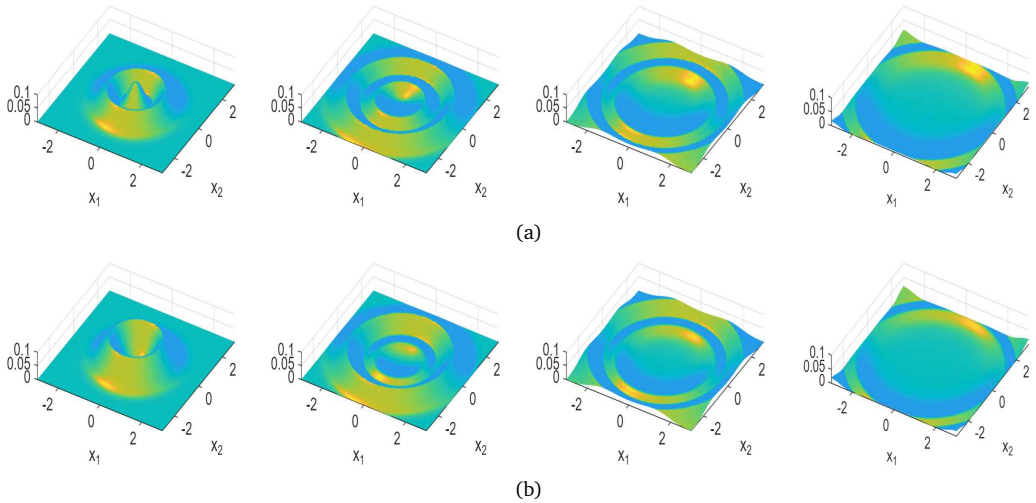

Figure 6: Case A. From left to right. Density functions at time $t = 1, 2, 3, 4$. (a) $|\Phi_1(x_1, x_2, t)|^2$. (b) $|\Phi_2(x_1, x_2, t)|^2$.

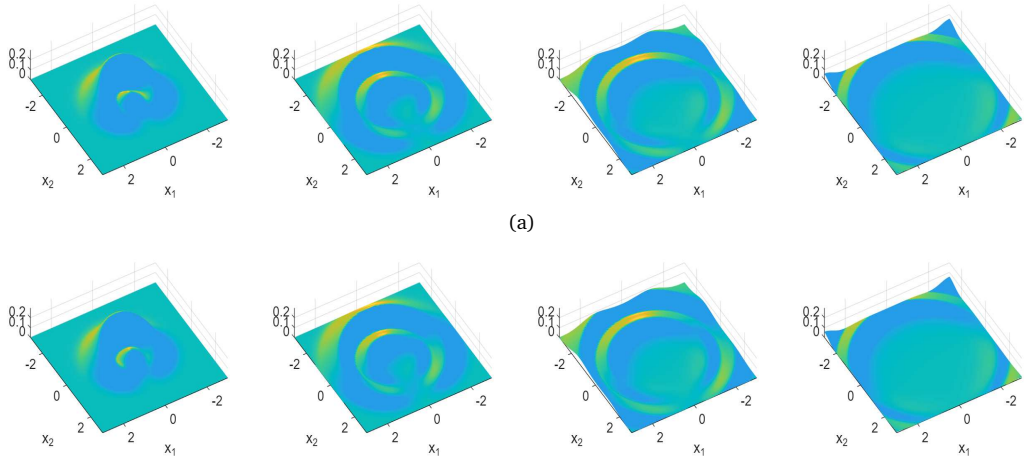

Figure 7: Case B. From left to right: Density functions at time $t = 1, 2, 3, 4$. (a) $|\Phi_1(x_1, x_2, t)|^2$, (b) $|\Phi_2(x_1, x_2, t)|^2$.

rings [17]. Moreover, we find an interesting result that the intensities of both $\Phi_1(x_1, x_2, t)$ and $\Phi_2(x_1, x_2, t)$ are two perfect rings and the width of the rings does not change.

In Fig. 7, initially, both $\Phi_1(x_1, x_2, t)$ and $\Phi_2(x_1, x_2, t)$ are Gaussian — i.e. Case B. Note that a spot becomes two bright rings, but the rings are not complete rings and they have notches at the bottom. The ring structures with notches are termed 'half turn of polarization around the ring', which has been predicted by Hamilton and been observed by Lloyd [35].

Figs. 6 and 7 show that the same evolution patterns as in lattice NLSE [3, 34], i.e. the rings expand radially with the same width of the ring under propagation with decreasing intensity. From them, we again illustrate that the tight-binding limit contains the underlying mechanism of conical diffraction in honeycomb lattices, and we can use the NLD system to describe the interesting phenomenon.

6. Conclusion

In this paper, we introduce the PML technique to the nonlinear Dirac equation, and propose a time-splitting Fourier-collocation method to solve the initial-boundary value problem for the nonlinear Dirac equation with PML. Coupled with the PML technique, the applied numerical method can absorb efficiently the reflections when the wave goes to the edges of the computational region. Moreover, with the help of our novel numerical method, the one-dimensional NLD equation with PML has been applied to simulate the dynamics of the soliton and the two-dimensional NLD equation with PML has been used to study the dynamical conical diffraction in honeycomb lattices. In the future, we plan to analyze the stability and convergence of the proposed numerical method.

Acknowledgements

D.W. thanks the Yunnan University of Finance and Economics for hosting her visit during 2024.

The research of H.W. is supported in part by the Natural Science Foundation of China (Grant Nos. 11871418, 12461081) and by the Yunnan Fundamental Research Projects (Grant No. 202101AS070044).

References

[1] D.A. Abanin et al., *Giant nonlocality near the Dirac point in graphene*, Science **332**(6027), 328–330 (2011).

[2] M.J. Ablowitz and J.T. Cole, *Nonlinear optical waveguide lattices: Asymptotic analysis, solitons, and topological insulators*, Phys. D **440**(15), Paper No. 133440 (2022).

[3] M.J. Ablowitz, S.D. Nixon and Y. Zhu, *Conical diffraction in honeycomb lattices*, Phys. Rev. A **79**(5), Paper No. 053830 (2009).

[4] M.J. Ablowitz and Y. Zhu, *Nonlinear waves in shallow honeycomb lattices*, SIAM J. Appl. Math. **72**, 240–260 (2012).

[5] A. Álvarez, P.Y. Kuo and L. Vázquez, *The numerical study of a nonlinear one-dimensional Dirac equation*, Appl. Math. Comput. **13**, 1–15 (1983).

[6] X. Antoine, F. Fillion-Gourdeau, E. Lorin and S. MacLean, *Pseudospectral computational methods for the time-dependent Dirac equation in static curved spaces*, J. Comput. Phys. **411**, 1–23 (2020).

[7] X. Antoine, C. Geuzaine and Q. Tang, *Perfectly matched layer for computing the dynamics of nonlinear Schrödinger equations by pseudospectral methods: Application to rotating Bose-Einstein condensates*, Commun. Nonlinear Sci. Numer. Simul. **90**, Paper No. 105406 (2020).

[8] X. Antoine and E. Lorin, *A simple pseudospectral method for the computation of the time-dependent Dirac equation with perfectly matched layers*, J. Comput. Phys. **395**, 583–601 (2019).

[9] X. Antoine, E. Lorin, J. Sater, F. Fillion-Gourdeau and A.D. Bandrauk, *Absorbing boundary conditions for relativistic quantum mechanics equations*, J. Comput. Phys. **277**, 268–304 (2014).

[10] X. Antoine, E. Lorin and Q. Tang, *A friendly review of absorbing boundary conditions and perfectly matched layers for classical and relativistic quantum waves equations*, Mol. Phys. **115**, 1861–1879 (2017).

[11] W. Bao and Y. Cai, *Mathematical theory and numerical methods for Bose-Einstein condensation*, Kinet. Rel. Models **6**(1), 1–135 (2013).

[12] W. Bao, Y. Cai, X. Jia and J. Yin, *Error estimates of numerical methods for the nonlinear Dirac equation in the nonrelativistic limit regime*, Sci. China Math. **59**(8), 1461–1494 (2016).

[13] W. Bao and X. Li, *An efficient and stable numerical method for the Maxwell-Dirac system*, J. Comput. Phys. **199**(2), 663–687 (2004).

[14] H. Bauke, H.G. Hetzheim, G.R. Mocken, M. Ruf and C.H. Keitel, *Relativistic ionization characteristics of laser-driven hydrogenlike ions*, Phys. Rev. A **83**(6), Paper No. 063414 (2011).

[15] J.P. Berenger, *A perfectly matched layer for the absorption of electromagnetic waves*, J. Comput. Phys. **114**(2), 185–200 (1994).

[16] J.P. Berenger, *Three-dimensional perfectly matched layer for the absorption of electromagnetic waves*, J. Comput. Phys. **127**(2), 363–379 (1996).

[17] M.V. Berry, *Conical diffraction asymptotics: Fine structure of Poggendorff rings and axial spike*, J. Opt. A **6**(4), 289–300 (2004).

[18] N. Bournaveas and G.E. Zouraris, *Split-step spectral scheme for nonlinear Dirac systems*, ESAIM Math. Model. Numer. Anal. **46**, 841–874 (2012).
[19] D. Brinkman, C. Heitzinger and P.A. Markowich, *A convergent 2d finite-difference scheme for the Dirac-Poisson system and the simulation of graphene*, J. Comput. Phys. **257**, 318–332 (2014).
[20] A.H. Castro Neto, F. Guinea, N.M.R. Peres, K.S. Novoselov and A.K. Geim, *The electronic properties of the graphene*, Rev. Mod. Phys. **81**, 109–162 (2009).
[21] R. Cheng, L. Wu, C. Pang and H. Wang, *A Fourier collocation method for Schrödinger-Poisson system with perfectly matched layer*, Commun. Math. Sci. **20**(2), 523–542 (2022).
[22] P.A.M. Dirac, *The quantum theory of the electron*, Proc. A **117**, 610–624 (1928).
[23] P.A.M. Dirac, *Principles of Quantum Mechanics*, Oxford University Press (1958).
[24] C.L. Fefferman and M.I. Weistein, *Honeycomb lattice potentials and Dirac points*, J. Amer. Math. Soc. **25**, 1169–1220 (2012).
[25] F. Fillion-Gourdeau, E. Lorin and A.D. Bandrauk, *Numerical solution of the Dirac equation and applications in laser-matter interaction*, AIP Conf. Proc. **1368**, 13–16 (2011).
[26] F. Fillion-Gourdeau, E. Lorin and A.D. Bandrauk, *Numerical solution of the time-dependent Dirac equation in coordinate space without fermion-doubling*, Comput. Phys. Commun. **183**(7), 1403–1415 (2012).
[27] F. Fillion-Gourdeau, E. Lorin and S. MacLean, *Numerical quasiconformal transformations for electron dynamics on strained graphene surfaces*, Phys. Rev. E **103**, Paper No. 013312 (2021).
[28] A. Gallerati, *Graphene properties from curved space Dirac equation*, Eur. Phys. J. Plus **134**, Paper No. 202 (2019).
[29] D.J. Gross and A. Neveu, *Dynamical symmetry breaking in asymptotically free field theories*, Phys. Rev. D **10**(10), 3235–3253 (1974).
[30] E. Hairer, C. Lubich and G. Wanner, *Geometric Numerical Integration*, Springer-Verlag (2006).
[31] J. Hong and C. Li, *Multi-symplectic Rung-Kutta methods for nonlinear Dirac equations*, J. Comput. Phys. **211**, 448–472 (2006).
[32] F.D.L. Hoz and F. Vadillo, *An integrating factor for nonlinear Dirac equations*, Comput. Phys. Commun. **181**, 1195–1203 (2010).
[33] D. Hsieh, D. Qian, L. Wray, Y. Xia, Y.S. Hor, R.J. Cava and M.Z. Hasan, *A topological Dirac insulator in a quantum spin hall phase*, Nature **452**, 970–974 (2008).
[34] R. Jiao, W. Zhang, Z. Yang, J. Wang, K. Zhan and B. Liu, *Conical diffraction modulation in honeycomb lattices*, Commun. Nonlinear Sci. Numer. Simul. **84**, Paper No. 105168 (2020).
[35] H. Lloyd, *On the phenomena presented by light in its passage along the axes of bi-axal crystals*, Trans. R. Irish Acad. **17**, 145–157 (1831).
[36] P. Mathieu and R. Saly, *Baglike solutions of a Dirac equation with fractional nonlinearity*, Phys. Rev. D **29**(12), 2879–2883 (1984).
[37] J.S. Pedernales, M. Beau, S.M. Pittman, I.L. Egusquiza, L. Lamata, E. Solano and A. del Campo, *Dirac equation in (1+1)-dimensional curved spacetime and the multiphoton quantum Rabi model*, Phys. Rev. Lett. **120**, Paper No. 160403 (2018).
[38] O. Pinaud, *Absorbing layers for the Dirac equation*, J. Comput. Phys. **289**, 169–180 (2015).
[39] U.W. Rathe, C.H. Keitel, M. Protopapas and P.L. Knight, *Intense laser-atom dynamics with the two-dimensional Dirac equation*, J. Phys. B: At. Mol. Opt. Phys. **30**(15), L531–L539 (1997).
[40] K. Schratz, Y. Wang and X. Zhao, *Low-regularity integrators for nonlinear Dirac equations*, Math. Comp. **90**, 189–214 (2021).
[41] S. Shao and H. Tang, *Higher-order accurate Runge-Kutta discontinuous Galerkin methods for a nonlinear Dirac model*, Discrete Contin. Dyn. Syst. B **6**, 623–640 (2006).
[42] M. Soler, *Classical, stable, nonlinear spinor field with positive rest energy*, Phys. Rev. D **1**(10), 2766–2769 (1970).

[43] W.E. Thirring, *A soluble relativistic field theory*, Annals Phys. **3**(1), 91–112 (1958).
[44] D. Wang, Y. Zhang and H. Wang, *A splitting spectral method for the nonlinear Dirac-Poisson equations*, Int. J. Numer. Anal. Model. **20**(4), 577–595 (2023).
[45] H. Wang and H. Tang, *An efficient adaptive mesh redistribution method for a nonlinear Dirac equation*, J. Comput. Phys. **222**(1), 176–193 (2007).
[46] J. Xu, S. Shao and H. Tang, *Numerical methods for nonlinear Dirac equation*, J. Comput. Phys. **245**, 131–149 (2013).
[47] H. Yoshida, *Construction of higher order symplectic integrators*, Phys. Lett. A **150**, 262–268 (1990).
[48] C. Zheng, *A perfectly matched layer approach to the nonlinear Schrödinger wave equation*, J. Comput. Phys. **227**, 537–556 (2007).